ELSEVIER

Contents lists available at ScienceDirect

Construction and Building Materials

journal homepage: www.elsevier.com/locate/conbuildmat





Strain sensing ability of GNP reinforced cementitious composites: The role of exfoliation and interlayer spacing

Panagiotis A. Danoglidis a, Maria S. Konsta-Gdoutos b,

- ^a Assistant Professor of Research, Center for Advanced Construction Materials, Department of Civil Engineering, The University of Texas at Arlington, 701 S Nedderman Dr, Arlington, TX 76019, United States
- b Associate Director of the Center for Advanced Construction Materials, Professor of Civil Engineering, The University of Texas at Arlington, 701 S Nedderman Dr, Arlington, TX 76019, United States

ARTICLE INFO

Keywords:
Graphene nanoplatelets
Exfoliation
Percolation threshold
Dielectric permittivity
Piezopermittivity
Cement-based materials

ABSTRACT

In this study, the effect of the exfoliation state of GNPs on the strain sensing capacity of GNP reinforced cementitious composites at the elastic and post-elastic stages of deformation is demonstrated. Below percolation threshold, effective exfoliation of multi-layer GNPs results in tri-layer nanomaterials. For GNP volume fractions above percolation a direct correlation between the number of exfoliated graphene layers and permittivity values of the cementitious nanocomposites exists. Electrochemical Impedance Spectroscopy (EIS) measurements demonstrated that the nanocomposite's electrical energy storage capacity depends on the interlayer spacing between graphene nanosheets. Piezoresistivity experiments showed that the piezoresistive signal is independent on the strain levels at the post-elastic stage. Piezopermittivity results revealed an excellent relationship between the fractional change in permittivity and stress and strain values during the loading–unloading cycles at both the elastic and post-elastic stages. A direct relationship between piezopermittivity and volume fraction of tri-layer and multi-layer GNPs is also observed suggesting that the GNP content at the percolation threshold is optimum for maximizing the strain sensing capacity of the nanocomposite.

1. Introduction

Graphene nanoplatelets (GNPs) are 2D nanomaterials with ultrahigh surface area, 500-2500 m²/g and hexagonal crystal lattice structure of carbon-carbon bonds (C-C) that exhibit extraordinary intrinsic electrical conductivity, orders of magnitude higher than that of 0D and 1D carbon-based nanomaterials [1,2]. The unique combination of intrinsic properties makes GNPs a prime candidate for developing functional cementitious nanocomposites with robust electromechanical strain sensing capacity [3,4]. Due to the lack of proper dispersion methods, research in nanoreinforced cementitious materials mainly focus on using high concentrations of stacked multi-layer GNPs [5]. Early attempts to evaluate the electrical properties and self sensing ability of cement pastes reinforced with stacked multi-layer GNPs, at volume fractions of 1.2–4.8 vol% were reported by Dai Pang et al. [6,7]. Compared to OPC pastes, the authors reported 2-3x higher electrical conductivity. However, the piezoresistive signal during compression and tension up to failure was deemed inadequate for self-sensing. Dong et al. [8] reported negligible piezoresistivity for cement pastes and

mortars reinforced with stacked multi-layer GNPs at a volume fraction of 1.5 vol%. Similar results (piezoresistive response of $\approx\!3\%$) were reported by Sun et al. [9] and Sevim et al. [10] for cementitious composites reinforced with stacked multi-layer GNPs at high volume fractions of 1.5–4 vol%. Recently, Qi et al. [11] reported that a low weight fraction of 0.2 wt% ($\approx\!0.4$ vol%) of GNPs with high thickness (100 nm) and diameter (20–45 μ m) defines the percolation threshold. Piezoresistivity tests under compressive and tensile load revealed that the fractional change in resistivity reaches a maximum at the percolation threshold and proportionally decreases for higher GNP dosages.

More recently, Kausar et al. [12] demonstrated that the electrome-chanical strain sensing ability depends on the GNPs' electron mobility. Fang et al. [13] used atomic-scale simulations of the electron density stored within the interlayer spacing between graphene nanosheets. They have shown that compared to stacked multi-layer GNPs, prepared by the commercial production methods, tri-, bi- and mono- layer GNPs exhibit much higher electron mobility. Robin et al. [14] conducted Scanning Tunneling Microscopy experiments to develop a Fermi level shift computation model and confirmed that the poor electron mobility of

E-mail address: maria.konsta@uta.edu (M.S. Konsta-Gdoutos).

^{*} Corresponding author.

stacked multi-layer GNPs is attributed to the interlayer spacing between the multiple graphene sheets that significantly lowers the nanomaterial's electron transport properties, namely electron mobility, charge surface density, carrier concentration, Fermi velocity, and Dirac Furthermore, the piezoresistive response of nanoelectromechanical membrane gauges with multi-layer GNPs revealed an independence of the multi-layer GNP loading and the fractional change in resistivity, for GNP concentrations above percolation threshold [15]. A comparison between the effect of various loadings of multi- and fewlayer GNPs on the piezoresistive behavior of 3D graphene-based sensors [16] revealed that few-layer GNP-based sensors exhibit a much higher sensing capability, and that fractional change in resistivity is independent on the GNP concentration. From all the above it is concluded that while the use of multi-layer GNPs can successfully enhance the electrical conductivity, yet the observed fractional changes in resistivity indicate that strain sensing does not depend on the volume fraction of stacked multi-layer GNPs. To successfully enhance the strain sensing ability, the focus is currently shifted on minimizing the energy storage capacity of the interlayer spacing by successfully exfoliating the stacked multi-layer GNPs into few-layer nanoplatelets.

In this study, the effect of the exfoliation state and volume fraction of GNPs on the electrical and dielectric properties, and resistivity- and permittivity- based strain sensing ability of GNP reinforced mortars is presented herein. Stacked multi-layer GNPs at several volume fractions were effectively exfoliated into few-layers, through a liquid-phase exfoliation process by applying ultrasonication energy at controlled rates. The number of graphene layers and the lateral dimension of GNPs were monitored via Raman spectroscopy. The electrical resistivity and dielectric permittivity of mortars reinforced with several volume fractions of exfoliated GNPs were evaluated using Electrochemical Impedance Spectroscopy (EIS) measurements. The piezoresistivity and piezopermittivity of GNP reinforced mortars subjected to cyclic compressive loading in the elastic and post-elastic stages were assessed. A direct relationship between the number of layers, the interlayer spacing, and dielectric permittivity is demonstrated for GNP loadings above percolation. A good correlation between the piezopermittivity values and the GNP volume fraction was observed suggesting that the optimum GNP content for strain sensing can be defined by the percolation threshold.

2. Materials and experimental procedure

2.1. Materials and specimen preparation

GNP reinforced mortars with water to cement ratio of 0.485 and sand to cement ratio of 2.75 were produced as per the ASTM C109/C109M – 20 [17]. Type I Portland Cement (OPC) 42.5 R was used as binder material. Standard sand as per the ASTM C778 [18] was used as a fine aggregate. Graphene nanoplatelets at volume fractions of 0.05%, 0.1%, 0.15%, 0.2%, 0.25%, 0.30%, 0.32%, 0.35%, 0.4%, 0.5%, 0.6%, and 0.7 vol% were used as electrically conductive materials. GNPs were manufactured through a non-oxidizing process to ensure a uniform graphitic surface of sp2 carbon molecules of each graphene layer, essential for applications that require high electrical conductivity [19]. The number of graphene layers, geometrical and physical properties, and intrinsic electrical conductivity of "as received" stacked multi-layer GNPs are shown in Table 1.

In this work, a simple, one step sonication procedure was applied to overcome the strong carbon–carbon van der Waals interactions and

homogeneously exfoliate the GNPs in the mixing water [20,21]. Suspensions were prepared by adding GNPs to an aqueous solution that includes a polycarboxylate based surfactant. The surfactant to nanoplatelet weight ratio was kept at 4.0 for all mixes. Ultrasonication energy was then applied to the suspensions by a 750 W cup-horn high intensity ultrasonic processor with a standard probe of a diameter of 19 mm and a temperature controller. The sonicator was operated at amplitude of 57% so as to deliver constant energy rate of $1.9-2.1 \cdot 10^3$ J/min, at cycles of 20 s in order to prevent overheating of the suspensions. After ultrasonication process, Zeta potential measurements were used to evaluate the stability of the dispersed/exfoliated nanomaterials in suspensions using the Zetasizer Nano ZS system [22]. Prior to sonication, suspensions exhibit values lower than 30 mV, which indicates unstable hydrophobic suspensions [23]. The Zeta potential of the GNP suspensions increases with the application of ultrasonication energy reaching a value of 42.5 mV which indicates an excellent stability for all suspensions.

The exfoliated GNP suspensions were then added into the OPC and sand, and mixing of the materials was performed according to the procedure outlined by ASTM C305 [24] using a standard robust mixer capable of operating from 140 \pm 5 revolutions per minute (r/min) to 285 \pm 10 r/min. After the completion of the procedure the mixture was cast in 40 \times 40 \times 160 mm^3 oiled molds. Two titanium grids 40 \times 60 mm^2 with a spacing of 100 mm between them were embedded in each specimen after casting for AC measurements. All specimens remained molded and sealed with plastic sheet for 24 h to prevent moisture evaporation. Following demolding, the specimens cured in a curing room at a temperature of 20 °C and 95% humidity for 28 days.

2.2. Experimental study

2.2.1. Characterization of the exfoliation state and number of layers of GNP-suspensions

Raman spectroscopy was used for the determination of the optimum amount of ultrasonication energy by evaluating the exfoliation state of GNP-suspensions subjected to ultrasonication energy at amounts of up to $4.0 \cdot 10^3$ kJ/L. The Raman spectra of GNP-suspensions were recorded using the Raman DXR3 spectrometer equipped with a microscope objective MPlan 10x/0.25. The samples were excited with laser beam of 532 nm wavelength before spectra recording. Raman scattered light was analyzed at a scanning wavelength of 1000-3200 cm⁻¹ using a diffraction grating (900 lines mm⁻¹) and a CCD camera. The actual number of layers of exfoliated GNPs at several volume fractions ranging from 0.05% to 0.7 vol% was determined using the intensity ratio of the 2D-peak and G-peak (I_{2D}/I_{G}) according to [25].

The complex impedance, namely resistance, Z', and absolute reactance, |Z''|, and the dielectric permittivity, ε , of the 28d GNP reinforced mortars were determined by EIS measurements over frequencies ranging from 20 Hz to 1 MHz following the AC two pole method [26]. As no standards exist, nine specimens of each sample of plain and GNP reinforced mortars were used for the EIS measurements.

The stress and strain sensing ability of the 28d GNP reinforced mortars was assessed by evaluating their fractional change in resistivity (piezoresistivity) and fractional change in permittivity (piezopermittivity) following the AC two pole method, while cyclic uniaxial compressive loading was simultaneously applied to the specimens at a rate of 0.84 MPa/s and frequency of 0.0083 Hz using an electromechanical testing machine MTS with a 500 kN capacity [27,28]. The magnitude of compressive loading was increased at stress intervals of 5 MPa up to specimen's compressive strength. Two loading–unloading

Table 1Properties of "as received" stacked multi-layer GNPs.

	Number of Layers	Thickness (nm)	1-Layer Thickness (Å)	d-spacing (Å)	Lateral Dimension (µm)	Surface area (m ² /g)	Electrical Conductivity (S/m)
GNPs	13–16	7–9	3.45	3.4	2	750	10^{6}

cycles were recorded for each stress level, and every cycle of loading–unloading had a duration of $120 \ \mathrm{s}.$

3. Results and discussion

3.1. Evaluation of the number of layers and exfoliation state of GNPs

Fig. 1 presents the Raman Intensity – Raman Shift of 0.3 vol% GNP suspensions subjected to ultrasonication energy up to 4.0 • 10³ kJ/L. The 0.3 vol% GNP loading was selected as the optimum volume fraction to maximize the electrical conductivity of GNP reinforced polymer nanocomposites [29]. Three prominent peaks are observed in Fig. 1 for all Raman Intensity - Raman Shift curves, namely the D-peak (~1345 cm^{-1}), G-peak ($\sim 1580 cm^{-1}$) and 2D-peak ($2685-2716 cm^{-1}$) [30]. The D-peak is attributed to the non-covalent bonding between carbon atoms, along the edge of exfoliated nanoplatelets, and hydroxyl and carboxyl groups from the polycarboxylate-based surfactant. The G-peak reflects the graphite band which arises from the stretching of the carbon-carbon (C-C) bond and corresponds to the crystallinity of graphene. The 2Dpeak is associated with the amount of sp² hybridized carbon atoms in graphene nanolayers. The Raman intensity of the three peaks is directly proportional to the exfoliation degree of GNPs and number of graphene layers. It is observed from Fig. 1 that the Raman intensity increases with increasing the ultrasonication energy, indicating a more effective exfoliation of the multi-layer GNPs. The position of the 2D-peak exhibits a shift from 2716 cm⁻¹ for the "as received" GNPs to 2685 cm⁻¹ for the exfoliated GNPs after the application to ultrasonication energy of 3.6 - $4.0 \cdot 10^3$ kJ/L. This shift is attributed to the elongation of sp² bonds of carbon atoms which results to the slippage of the graphene layers during ultrasonication; hence to the higher exfoliation state of GNPs [31]. The actual number of graphene layers in exfoliated GNPs can be determined using the intensity ratio of the 2D-peak and G-peak (I_{2D}/I_G) [25] following the equation:

$$N = 0.14 \left(\frac{I_{2D}}{I_G}\right)^{-4.62} \tag{1}$$

The number of graphene layers, N, of GNPs subjected to ultrasonication energy of 0.6– $4.0 \cdot 10^3$ kJ/L is presented in Fig. 2. The number of layers of "as received" stacked multi-layer GNPs, calculated by Eq. (1) using the Raman intensity data is ~15 and falls within the range of the number of layers given by the manufacturer (Table 1). Increasing the ultrasonication energy for amounts up to $3.6 \cdot 10^3$ kJ/L

proportionally increases the exfoliation state of multi-layer GNPs resulting in up to 3 graphene layers. It is also observed from Fig. 2 that application of higher than $3.6 \cdot 10^3$ kJ/L ultrasonication energies does not reduce further the number of graphene layers.

A qualitative evaluation of the exfoliation state of GNPs was performed by scanning electron microscopy (SEM) using an ultra-high resolution field emission scanning electron microscope (Hitachi SU 3800), operated at 3 kV. Fig. 3a shows the "as received" GNPs with 15 layers of stacked graphene sheets before sonication. An individual trilayer GNP was identified in the aqueous GNP/surfactant suspension after the application of ultrasonication energy of $3.6 \cdot 10^3$ kJ/L (Fig. 3b).

The successful exfoliation of multi-layer GNPs into a few-layer nanomaterial requires a controlled application of ultrasonication energy that ensures the preservation of GNP's lateral dimension, L. The GNP's lateral dimension can be calculated using the intensity values of the D-peak (I_D) and G-peak (I_G) [25] following the equation:

$$L = \frac{0.14}{(I_D/I_G)_{GNP} - (I_D/I_G)_{Graphite}}$$
 (2)

Where $(I_D/I_G)_{GNP}$ is the ratio of the I_D and I_G observed in the Raman spectra of exfoliated GNPs (Fig. 1) and $(I_D/I_G)_{Graphite}$ is the ratio for pure graphite [32].

The lateral dimension values of exfoliated GNPs in suspensions subjected to ultrasonication process at energies up to $4.0 \bullet 10^3$ kJ/L are presented in Fig. 4. As shown in Fig. 4 maintaining the lateral dimension of exfoliated GNPs at $\sim\!2~\mu m$ (nominal lateral dimension value provided by the GNP manufacturer, Table 1) requires the application of ultrasonication energy at amounts up to $3.6 \bullet 10^3$ kJ/L. Ultrasonication energies higher than the optimum interrupt the GNP's structural integrity and result in lower lateral dimensions, 19% for $3.8 \bullet 10^3$ kJ/L and 30% for $4.0 \bullet 10^3$ kJ/L, respectively, probably due to high disorder degree of carbon atoms at the edges of GNPs that lead to the fragmentation of the graphene layers [33].

The number of graphene layers in suspensions with GNPs at volume fractions ranging from 0.05% to 0.7 vol%, as calculated by Eq. (1) using the I_{2D}/I_G ratios from Raman spectroscopy, are presented in Fig. 5. The GNP-suspensions were subjected to ultrasonication energy of $3.6 \cdot 10^3$ kJ/L. For loadings up to 0.3 vol% the I_{2D}/I_G ratio of the GNP suspensions is \sim 0.585 and corresponds to tri-layer GNPs. Increasing the GNP volume fraction proportionally decreases the I_{2D}/I_G ratio from \sim 0.585 to \sim 0.373. It is observed that the number of graphene layers proportionally increases as well from 3 up to 13 layers. It is concluded that at

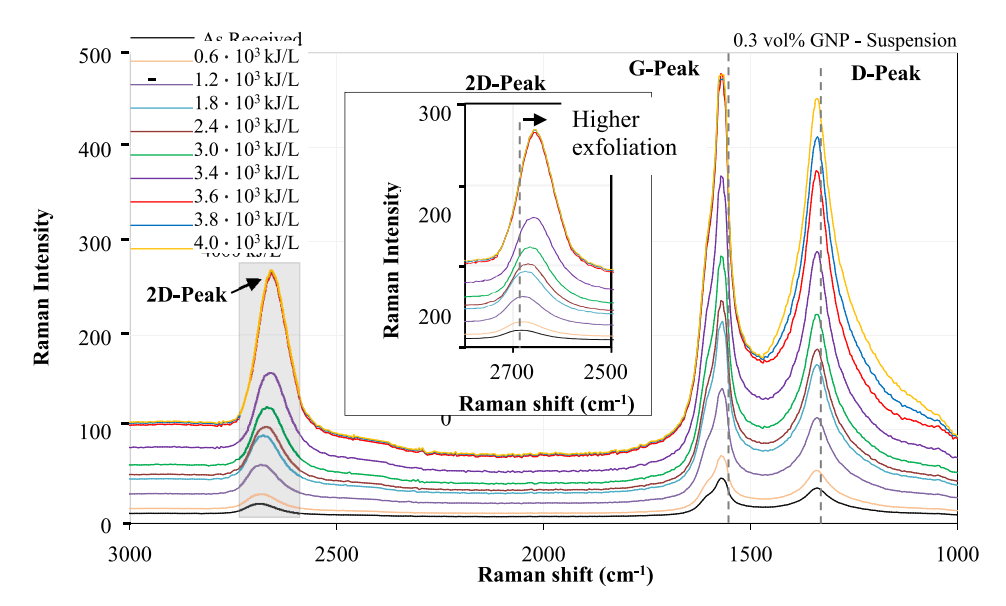


Fig. 1. Raman spectra of 0.3 vol% GNP-suspension as a function of ultrasonication energy.

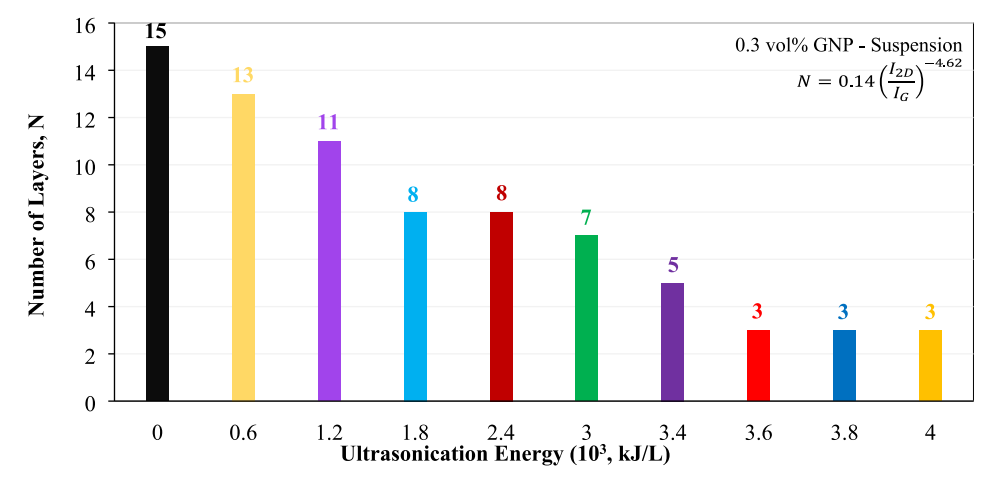


Fig. 2. Number of layers (*N*) of exfoliated 0.3 vol% GNPs as a function of ultrasonication energy.

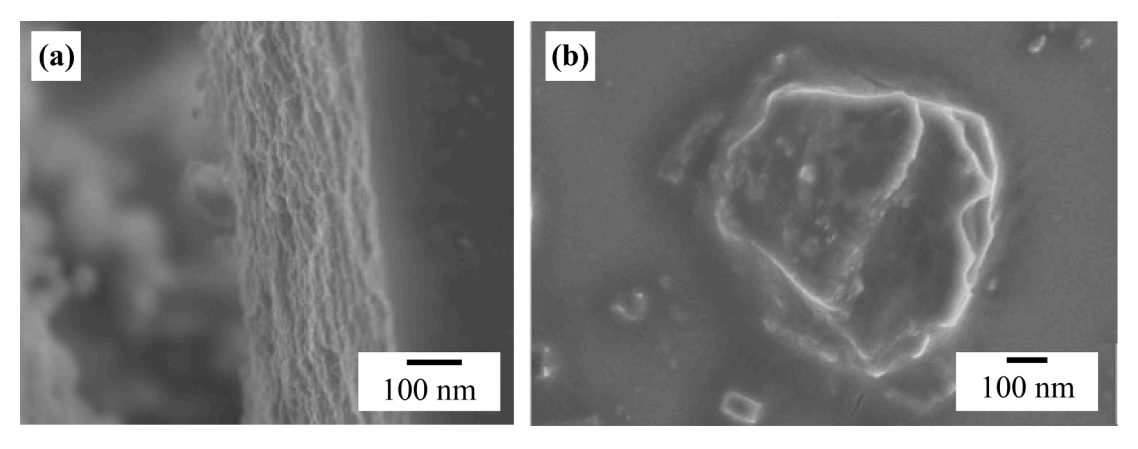
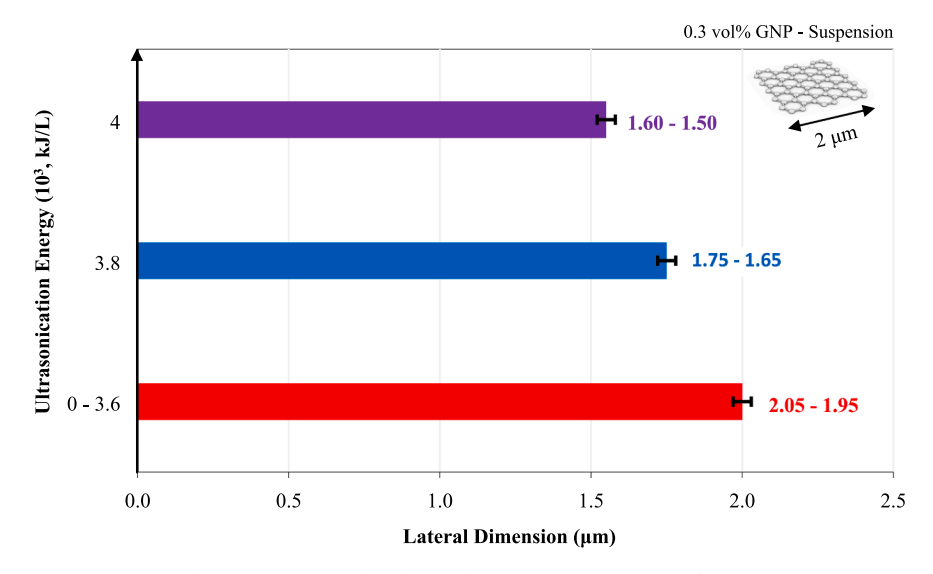


Fig. 3. SEM images of (a) "As received" GNPs with 15 layers of stacked graphene sheets and (b) individual exfoliated tri-layer GNP in the aqueous GNP/surfactant suspension.



 $\textbf{Fig. 4.} \ \ \textbf{Lateral Dimension of exfoliated 0.3 vol\% GNPs as a function of ultrasonication energy.}$

volume fractions between 0.32 and 0.7 vol% exfoliation is not complete and leads to multi-layer (>3) graphene inclusions.

3.2. Electrical resistivity and dielectric permittivity of GNP reinforced mortars

The complex impedance diagrams (Nyquist plots) of mortars reinforced with tri-layer GNPs at loadings from 0.05% to 0.7 vol% are

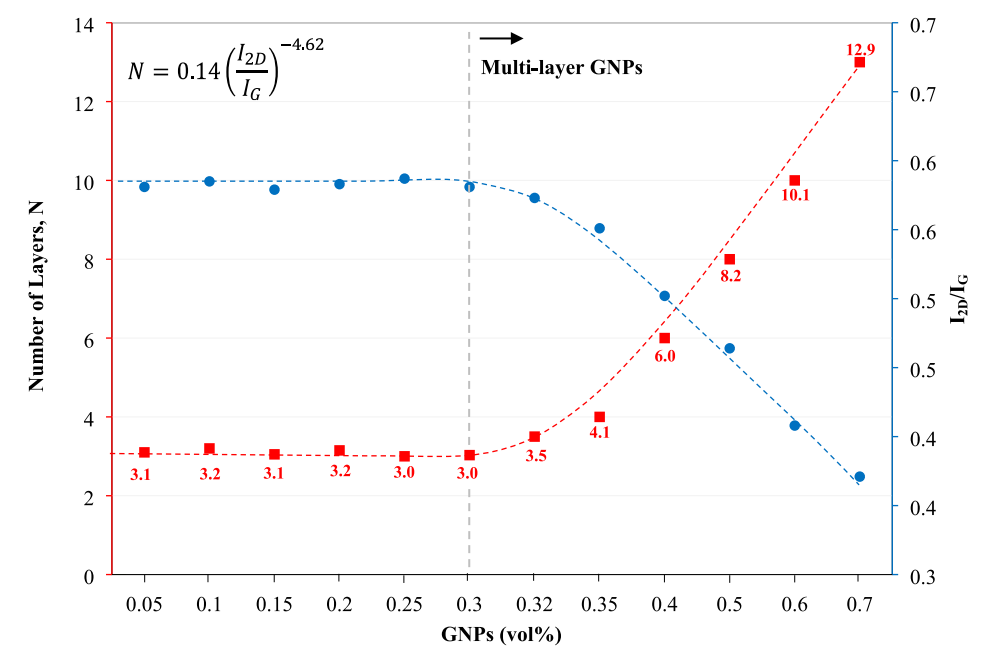


Fig. 5. Number of Layers (N) and I_{2D}/I_G ratio of exfoliated GNPs at a volume fraction range of 0.05% - 0.7 vol%.

presented in Fig. 6. The horizontal and vertical axes represent the real, Z', and the absolute imaginary part of impedance, |Z''|, respectively. The real part of impedance expresses the charge transfer resistance, also known as electrical resistance, and is inversely proportional to the rate of electron mobility. The imaginary part of impedance, expressed as values of absolute reactance, is associated with the electric charge storage capacity. Nyquist plots for cementitious nanocomposites are typically composed of two arcs: (i) the high frequency arc (100 kHz-1 MHz) which is associated with the bulk properties of the nanocomposite; and (ii) the low frequency arc (20 Hz-100 kHz), associated with the titanium electrode-specimen interface properties [26]. The low- and high-frequency arcs intersect at point (A) at 100 kHz and is known as the cusp point. At this frequency the material acts as a neat resistor, without exhibiting any energy storage capacity (Z'' = 0). The maximum value of absolute |Z''| at the high-frequency arc arises at 300 kHz (point B). This is the point where the material exhibits its highest storage

capacity of electrical energy. It is observed from Fig. 6 that the real part of the nanocomposites' impedance decreases with increasing GNP concentration up to 0.3 vol%, due to the gradual formation of a continuous conducting graphene network that facilitates the electron mobility along the interconnected GNPs. As a result, the electrical conductivity of the mortars reinforced with tri-layer GNPs increases up to 187% compared to plain mortar.

It can also be observed from Fig. 6 that the imaginary part of the impedance (reactance) decreases with increasing GNP concentrations up to 0.3 vol%; hence the stored electric energy in the nanocomposites diminishes across the GNP mortar mixes. The lowest bulk reactance value $|Z''_{300kHz}|=468~\Omega$ was observed for the 0.3 vol% GNP-mortar. Typically, the lowest bulk reactance values correspond to a state of a minimum electrical energy storage capacity of the mix. In this sense, the 0.3 vol% GNP-mortar is believed to have undergone perfect dispersion; therefore, it exhibits a uniform and homogenous distribution of the tri-

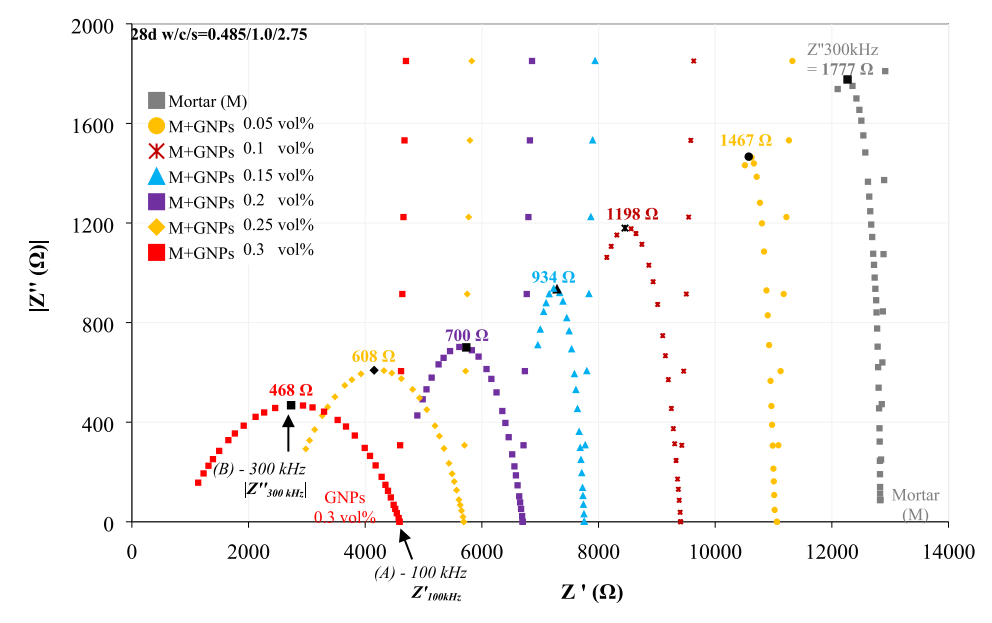


Fig. 6. Nyquist plots of 28d mortar reinforced with GNPs at volume fractions of 0.05-0.3 vol%.

layer graphene nanoplatelets within the cementitious matrix.

As already discussed in Section 3.1, GNPs at volume fractions > 0.3 vol% are considered multi-layered, i.e., 4-13 layers (Fig. 5). The Nyquist plots of mortars reinforced with GNPs at volume fractions of 0.32%, 0.35%, 0.4%, 0.5%, 0.6% and 0.7 vol% are presented in Fig. 7. Interestingly, it is observed that all mixes show the same bulk resistance value (measured at cusp point, 100 kHz), $Z'_{100kHz} = 4370 \Omega$. Since volume fractions > 0.3 vol\% correspond to the percolation threshold, it is assumed that above percolation, the bulk electrical conductivity of the nanocomposites is independent of the multi-layer GNP content. On the other hand, the reactance values (measured at the high frequency arc, 100 kHz-1 MHz), which represent the bulk electrical energy storage capacity of the nanocomposites, proportionally increase with the GNP content. Due to the incomplete dispersion in the cementitious matrix, these multi-layer GNPs act as stacked double layer capacitors, in the form of graphene layer/interlayer spacing/graphene layer, similar to that of metal/dielectric/metal [34]. The presence of stacked multi-layer GNPs therefore leads to a much higher volume of interlayer spacing within the matrix which increases the electrical energy storage capacity of the nanocomposites. It is observed in Fig. 7 that increasing the GNP content proportionally increases the number of layers, hence the volume of interlayer spacing into the cementitious material, leading to enhancements of the nanocomposites' dielectric permittivity by 20-200%.

The electrical resistivity, ρ , of the GNP reinforced mortars can be calculated using the electrical resistance values at 100 kHz, $Z'_{100\text{kHz}}$ (where the material acts as a neat resistor) by the following equation [26,35]:

$$\rho = Z'_{100kHz} \bullet \frac{S}{L} \tag{3}$$

where S is the cross section of the specimen, and L the distance between the two electrodes.

The nanocomposite's bulk maximum energy storage capacity is represented by the dielectric permittivity, ε . The dielectric permittivity is a true material property and can be calculated by the following equation [36]:

$$\varepsilon = \frac{\left|Z_{300kHz}''\right|}{\sqrt{Z_{300kHz}^2 + Z_{300kHz}''}^2} \bullet \frac{S}{L} \bullet \frac{\varepsilon_0}{\omega \bullet c_0}$$

$$\tag{4}$$

Where Z''_{300kHz} is the reactance values obtained by the Nyquist plots (Figs. 6 and 7), ε_0 is the permittivity of vacuum, ω is the angular frequency and ε_0 is the speed of light in vacuum.

The electrical resistivity and dielectric permittivity results of the GNP-mortars at volume fractions of 0.05% to 0.7 vol% are presented in Fig. 8. As discussed above, the incorporation of up to tri-layer GNPs into the cementitious matrix enhances the electron mobility along the conductive network; hence both the electrical resistivity and dielectric permittivity of mortars reinforced with GNPs up to percolation threshold (0.05% - 0.3 vol%) decrease with increasing the GNP loading. Above percolation threshold, the values of the electrical resistivity are independent of the GNP content and reach a plateau. This may be attributed to a selective electron transport pathway along the continuously interconnected GNPs. A different trend is observed for the dielectric permittivity of the GNP-mortars above percolation threshold, where the permittivity values increase proportionally with the GNP volume fractions. The increased dielectric permittivity observed in the GNP mortars for volume fractions > 0.3 vol% is the result of the higher amounts of the electrical energy stored in the interlayer spacing between the multiple graphene layers in stacked GNPs. Please note that interlayer spacing is directly proportional to the graphene layers: stacked GNPs with multiple graphene layers include larger volume of interlayer spacing.

3.3. Strain sensing ability of GNP reinforced mortars

The strain sensing ability of cementitious composites is typically expressed as the fractional change in resistivity under the application of mechanical loading. This is also known as piezoresistivity [37,38]. It was reported that for composites reinforced with 2D nanomaterials, such as graphene, the energy storage capacity of the interlayer spacing between the graphene layers of GNPs plays an important role on the electron mobility through the conductive network formed within the matrix [39]. Results presented in Section 3.2 show that the resistivity is independent of the GNP loading above percolation, while the dielectric permittivity proportionally increases with increasing GNP loading (Fig. 8). In this sense, the resistivity values above percolation are not able to provide any information on the material's response to applied stress. The fractional change of dielectric permittivity, a.k.a. piezopermittivity, on the other hand may serve as a better indicator of the material's sensing ability as the permittivity values essentially correspond to the change in the amount of the stored electrical energy in the nanocomposite [40].

3.3.1. Piezoresistivity-based sensing of GNP reinforced mortars Piezoresistivity results of 28d mortar reinforced with the tri-layer

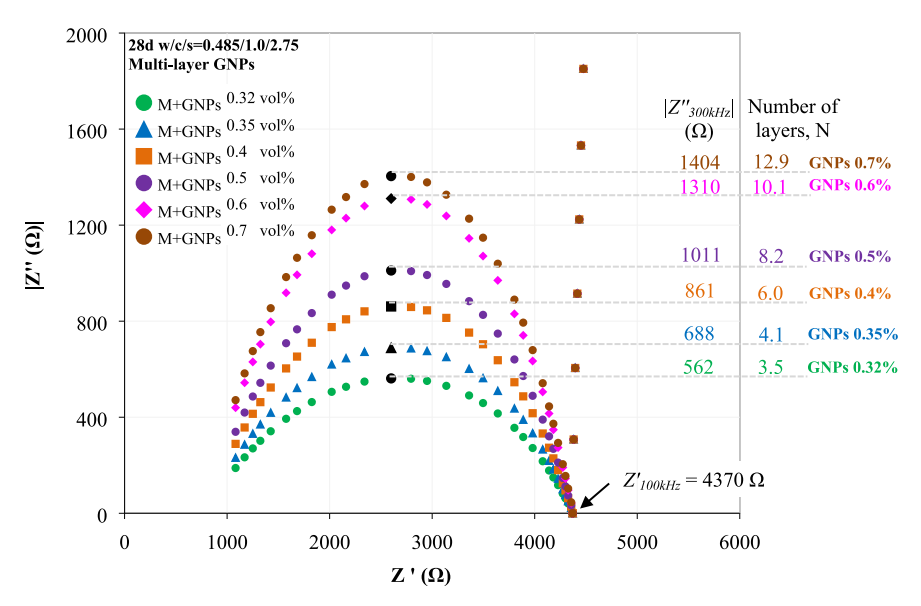


Fig. 7. Nyquist plots of 28d mortar reinforced with multi-layers GNPs at volume fractions of 0.3-0.8 vol%.

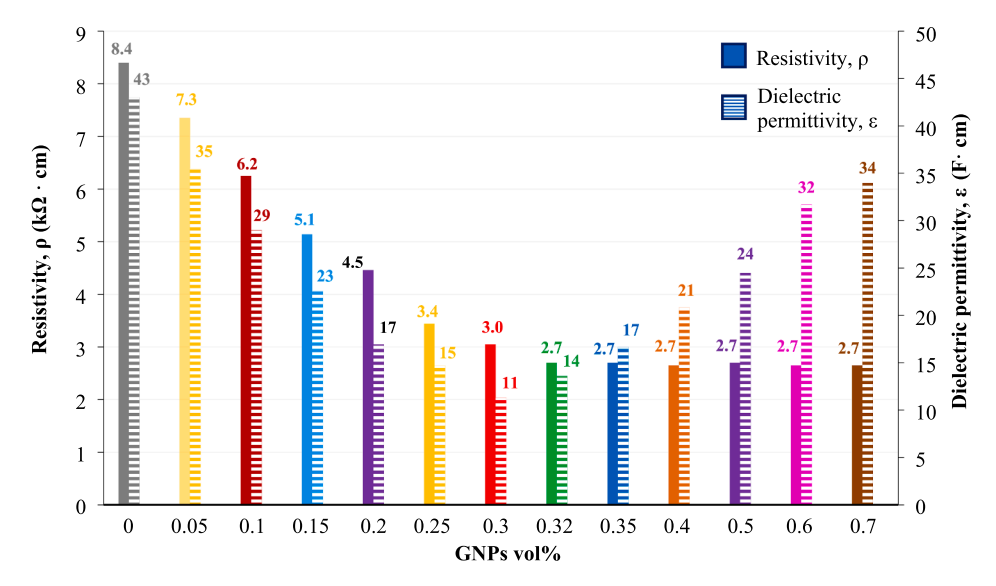


Fig. 8. Electrical resistivity, ρ , and dielectric permittivity, ε , of 28d mortar reinforced with GNPs at volume fractions of 0.05–0.7 vol%.

GNPs at 0.3 vol% (percolation threshold) are presented in Fig. 9. Compressive stress and strain during the loading and unloading cycles are expressed in normalized values. In a typical loading–unloading cycle, the fractional change in resistivity, $\Delta\rho/\rho_0$, decreases during loading and increases during unloading. It is observed that mortar reinforced with the exfoliated tri-layer GNPs was able to successfully follow the change in the applied stress, indicating a reversible piezoresistive response. The fractional change in resistivity, $\Delta\rho/\rho_0$, of the mortar prepared with "as received" GNPs is also included for

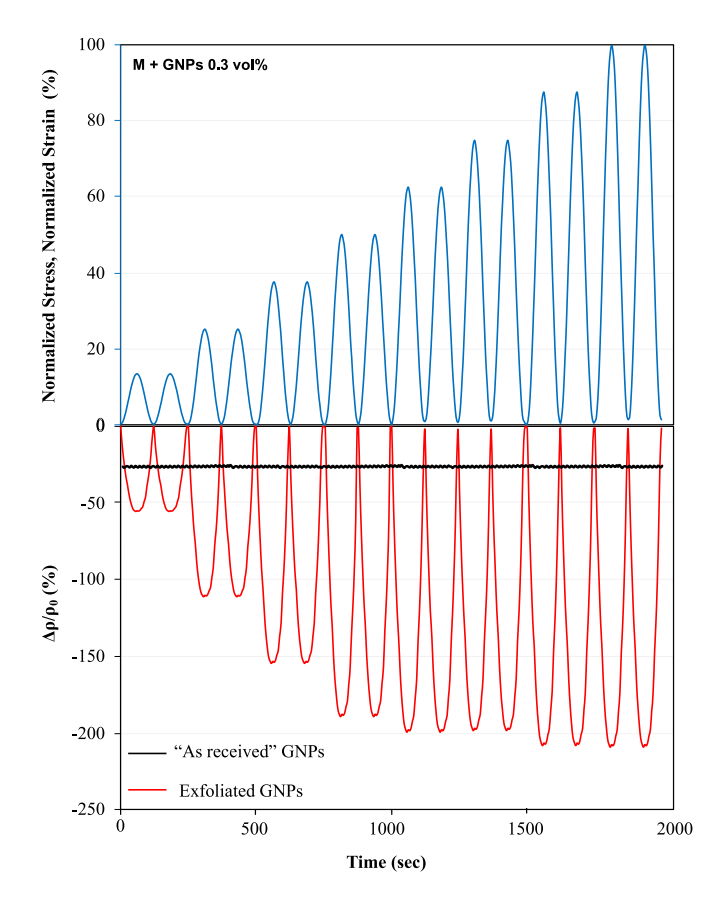


Fig. 9. Piezoresistivity, $\Delta\rho/\rho_0$, and normalized stress/strain curves of "as received" and exfoliated tri-layer 0.3 vol% GNP reinforced mortars.

comparison. It is observed that no sensing ability was detected for the "as received" GNP-mortar.

The fractional change in resistivity as a function of the specimen's strain for 28d mortars reinforced with exfoliated GNPs at loadings of 0.05% - 0.7 vol% are presented in Fig. 10. All nanomodified mortars exhibit an amplified ability to recognize the changes in their mechanical deformation through the recorded changes in the resistivity values. It is observed that for the tri-layer GNP mixes (0.05% - 0.3 vol%) the fractional change in resistivity, $\Delta\rho/\rho_0$, increases with the GNP content at all stress levels in both elastic and post-elastic stages, up to fracture. Increasing the GNP loading up to percolation threshold (0.3 vol%) proportionally increases the piezoresistive signal at a rate of 15% at all strain values. This is not the case for mortars reinforced with multi-layer GNPs above the percolation threshold (0.32% - 0.7 vol%). While the fractional change in resistivity observed for all mixes is considered adequate for strain sensing ($\Delta \rho / \rho_0 > 5\%$ [37]), yet the resistivity values have reached a plateau (Fig. 7) and the fractional change in resistivity demonstrates an independence on the GNP content for GNP loadings above percolation; hence the piezoresistive signal is not sensitive to the GNP volume fraction above percolation.

$3.3.2. \ \textit{Piezopermittivity-based sensing of GNP reinforced mortars}$

Fig. 11 presents the piezopermittivity, $\Delta \varepsilon/\varepsilon_0$, of the 28d mortars reinforced with tri-layer GNPs at 0.3 vol%. During the compressive loading–unloading cycles in the elastic and post-elastic stages the piezopermittivity increases proportionally with the increasing stress level, reaching a final fractional change in permittivity value of \approx 410%. Comparing with the piezoresistive response (Fig. 10), where the fractional change in resistivity demonstrates an independence on the stress levels at the post-elastic stage, it is observed that piezopermittivity allows for efficient monitoring of the stress and strain changes during loading–unloading at both elastic and post-elastic stages.

The fractional change in permittivity values as a function of the specimens' strain for 28d mortars reinforced with GNPs at 0.05%-0.7 vol% volume fractions are presented in Fig. 12. It is observed that all GNP reinforced mortars exhibit an enhanced ability to detect strain changes at all stages of deformation (elastic and post-elastic stages) through the fractional changes of dielectric permittivity. For volume fractions up to percolation threshold (0.3 vol%), increasing the GNP loading proportionally increases the piezopermittivity at a rate of $\approx\!40\%$ at all strain values for stress levels in both elastic and post-elastic stages, up to fracture. 0.3 vol% GNP-mortars outperform all other mixes, exhibiting the highest increase of piezopermittivity signal, 425% at

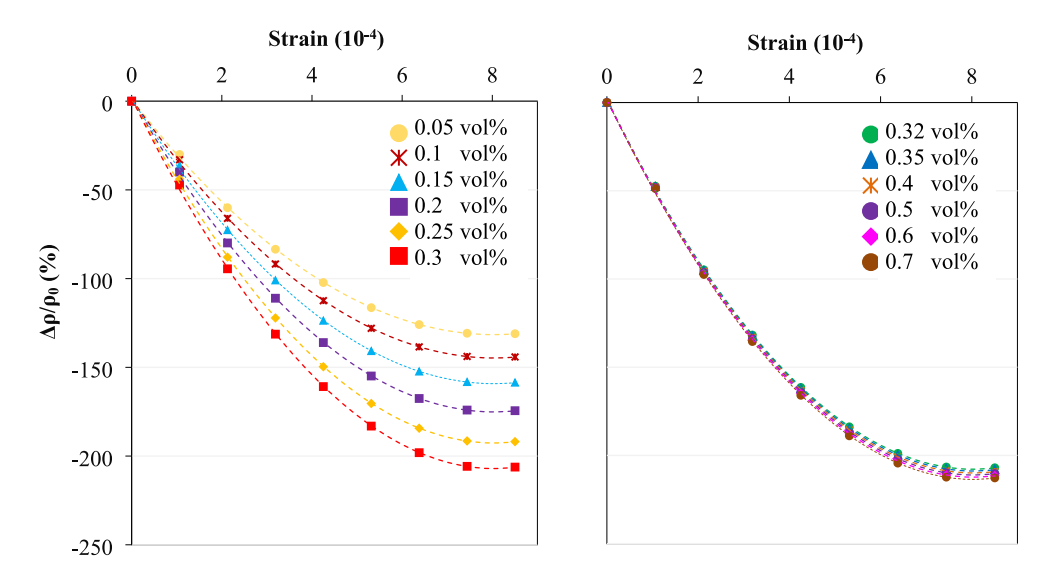


Fig. 10. Fractional change in resistivity, $\Delta \rho / \rho_0$, to strain correlation of 28d mortars reinforced with GNPs at volume fractions of 0.05% - 0.7 vol%, at all stress levels in both elastic and post-elastic stages, up to fracture.

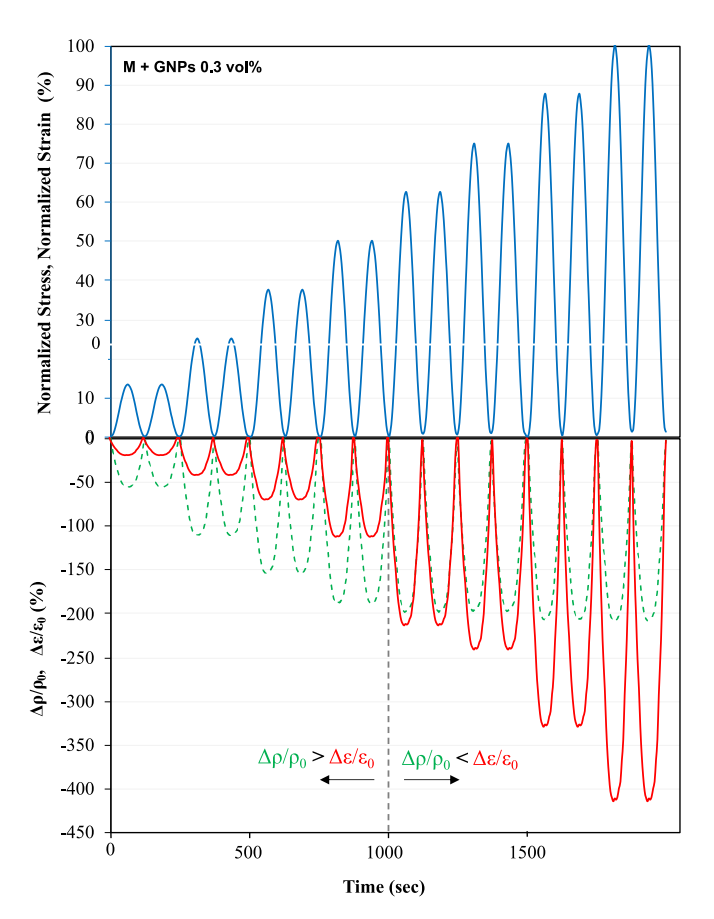


Fig. 11. Piezopermittivity, piezoresistivity and normalized stress/strain curves of 0.3 vol% GNP reinforced mortar.

fracture. A different pattern is observed for the composites reinforced with GNPs at volume fractions above percolation threshold (0.32% - 0.7 vol%), as the fractional change in permittivity decreases with increasing the GNP content. Compared to the 0.3 vol% GNP-mortars, mortars reinforced with 0.7 vol% GNPs exhibit $\Delta\epsilon/\epsilon_0$ values $\approx\!2x$ lower at all strain values, despite the < 2x higher GNP volume fraction. This is probably attributed to the presence of stacked multi-layer GNPs

that act as double layer capacitors with high electrical energy storage capacity, increasing the dielectric permittivity of the nanocomposite. It is observed that increasing the GNP dosages > 0.3 vol%, the number of graphene layers is also increased due to incomplete exfoliation process. The number of graphene layers is directly proportional to the volume of interlayer spacing; therefore, more graphene layers produce larger volumes of interlayer spacing that are able to store higher amounts of electrical energy. In general, interlayer spacing is considered a barrier that obstructs the electron mobility; hence a reduced permittivity-based strain sensing signal is observed in stacked multi-layer GNPs with larger volumes of interlayer spacing [38].

It should be noted here that piezopermittivity results could have been predicted, simply by examining the Nyquist plots at different stress levels. As discussed in Section 3.2, the bulk electrical energy storage capacity of the nanocomposite is represented by the absolute reactance value |Z''300kHz|. Permittivity values are calculated using the absolute reactance values at 300 kHz (Section 3.2, Eq. (4). Changes in absolute reactance values observed at different stress levels are directly related to the piezopermittivity values (Fig. 12) and reflect to the changes in the bulk electrical energy storage capacity of the material. As an example, we plotted the Nyquist plots of the 0.3% and 0.7 vol% GNP-mortars at two different stress levels, 0% and 100% (fracture), and compared their absolute reactance values at the frequency of 300 kHz ($|Z''_{300kHz}|$) (Fig. 13). The compressive strength to strain curves of the 28-day OPC mortar and mortars reinforced with GNPs 0.3% and 0.7 vol%, showing the 0% and 100% stress levels are also presented in Fig. 14. It is observed that the change in reactance values $|\Delta Z''_{300kHz}|$, between 0% and 100% stress, for both mixes, 0.3% and 0.7 vol% GNPs, are in perfect agreement with the piezopermittivity results presented in Fig. 12. These results confirm that compared to the multi-layer GNPs, well exfoliated tri-layer GNPs exhibit lower energy storage capacity of the interlayer spacing and high electron mobility. In composites reinforced with 2D nanomaterials, such as graphene nanoplatelets, interlayer spacing and high electron mobility is the key for strong sensing properties; hence proper exfoliation of stacked GNPs into few-layers is necessary to enhance the strain sensing signal.

4. Conclusions

In this study, the effect of the exfoliation state of GNPs on the electrical conductivity, dielectric properties and strain sensing capacity of GNP reinforced cementitious composites at the elastic and post-elastic

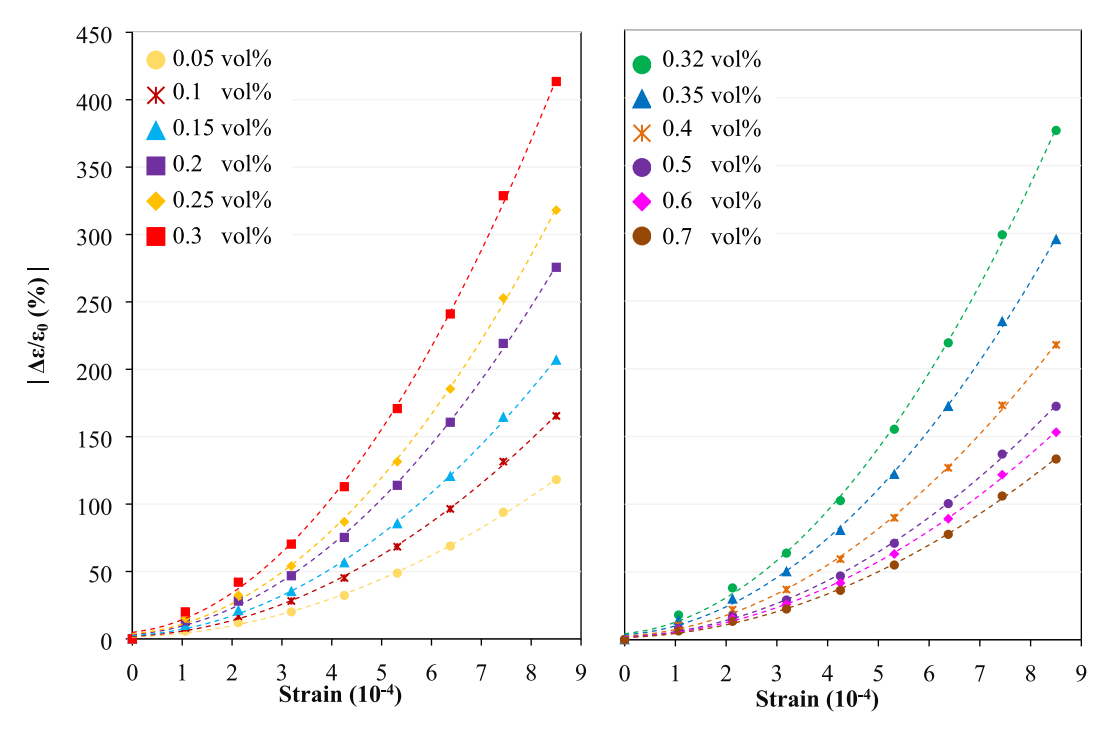


Fig. 12. Fractional change in permittivity, $\Delta\epsilon/\epsilon_0$, to strain correlation of 28d mortars reinforced with GNPs at volume fractions of 0.05% - 0.7 vol%, at all stress levels in both elastic and post-elastic stages, up to fracture.

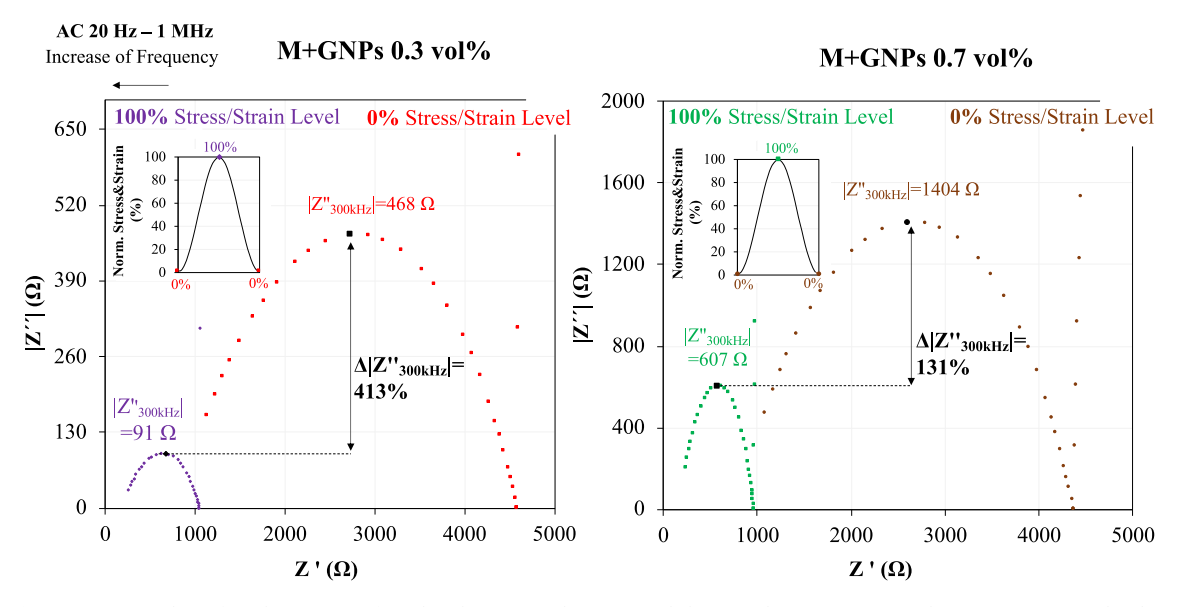


Fig. 13. Nyquist plots of 28-d mortar reinforced with (a) 0.3 vol% GNPs and (b) 0.7 vol% GNPs at 0% and 100% stress/strain levels.

stages of deformation is demonstrated. Raman spectroscopy analysis revealed that the controlled application of ultrasonication energy of $3.6\cdot 10^3~\rm kJ/l$ exfoliates the multi-layer GNPs into tri-layer graphene nanosheets and preserves the 2D nanomaterial's structural integrity, while higher energies interrupt the GNP's lateral dimensions due to high disorder degree of carbon atoms at the edges of GNPs that lead to the fragmentation of the graphene layers. EIS experiments showed that, compared to the multi-layer GNPs, well exfoliated tri-layer GNPs exhibit lower energy storage capacity. Above percolation threshold the bulk electrical conductivity of the nanocomposites is independent of the multi-layer GNP content. On the other hand, dielectric permittivity, which represent the bulk electrical energy storage capacity of the nanocomposites, proportionally increases with the GNP content due to

the presence of stacked multi-layer GNPs which act as double graphene layer capacitors, able to store high amounts of electrical energy.

Mortars reinforced with GNPs at volume fractions below and above percolation threshold exhibit a strong piezoresistivity-based sensing signal, within the elastic stage. However, the signal is not sensitive to strain values at stress levels in the post-elastic stage. Contrary to the piezoresistivity-based sensing signal, the signal based on the dielectric properties (piezopermittivity) allows for efficient monitoring of the stress and strain changes during loading–unloading at both elastic and post-elastic stages. Therefore, piezopermittivity-based sensing signal serves as a better indicator of the material's sensing ability as the permittivity values essentially correspond to the change in the amount of the stored electron molecules in the graphene layers of GNPs. In

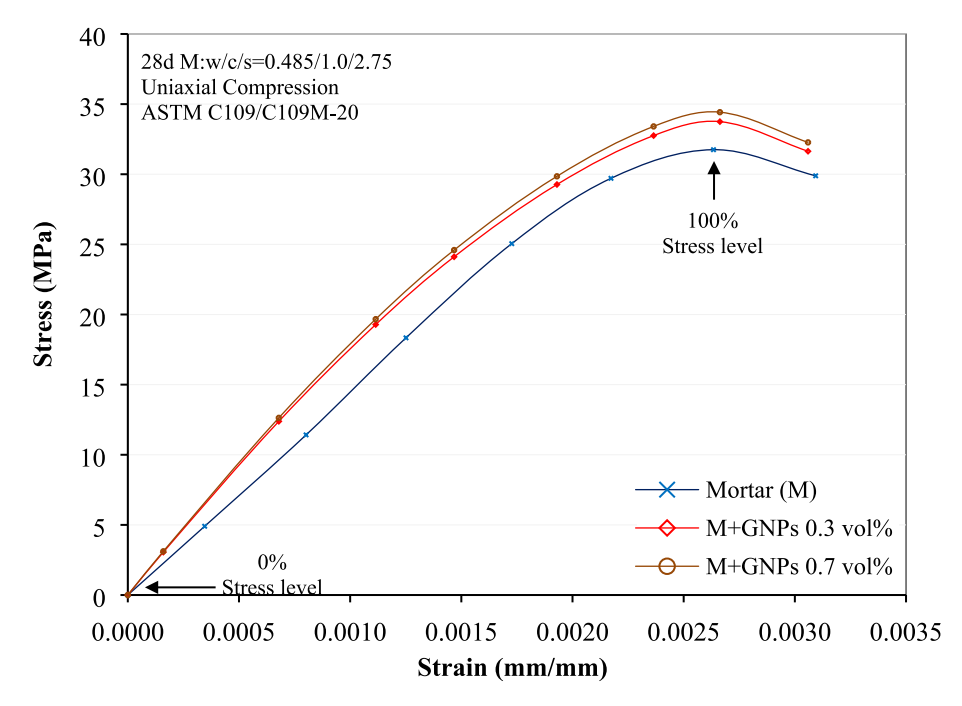


Fig. 14. Compressive stress to strain curves of 28-d plain mortar and mortars reinforced with 0.3% and 0.7 vol% GNPs.

composites reinforced with 2D nanomaterials, such as graphene nanoplatelets, the control and modification of electrical energy stored within the interlayer spacing of graphene sheets is the key for strong sensing properties; hence proper exfoliation of stacked GNPs into few-layers is necessary to enhance the strain sensing signal.

CRediT authorship contribution statement

Panagiotis A. Danoglidis: Conceptualization, Methodology, Validation, Investigation, Writing – review & editing, Formal analysis, Writing – original draft, Data curation. **Maria S. Konsta-Gdoutos:** Conceptualization, Methodology, Validation, Writing – review & editing, Funding acquisition, Supervision, Project administration, Resources.

Declaration of Competing Interest

The authors declare that they have no known competing financial interests or personal relationships that could have appeared to influence the work reported in this paper.

Data availability

Data will be made available on request.

Acknowledgments

The authors would like to acknowledge the financial support of the National Science Foundation-Partnerships for International Research and Education (PIRE) Research Funding Program "Advancing International Partnerships in Research for Decoupling Concrete Manufacturing and Global Greenhouse Gas Emissions" (NSF PIRE-2230747). The help provided by the Ph.D. students at the Center for Advanced Construction Materials of The University of Texas at Arlington, Myrsini Maglogianni and Michail Margas, is greatly appreciated.

References

- A. Alatawna, M. Birenboim, R. Nadiv, M. Buzaglo, S. Peretz-Damari, A. Peled, O. Regev, R. Sripada, The effect of compatibility and dimensionality of carbon nanofillers on cement composites, Constr. Build. Mater. 232 (2020) 117141.
- [2] H. Yang, H. Cui, W. Tang, Z. Li, N. Han, F. Xing, A critical review on research progress of graphene/cement based composites, Compos. A Appl. Sci. Manuf. 102 (2017) 273–296.
- [3] Z. Tian, Y. Li, J. Zheng, S. Wang, A state-of-the-art on self-sensing concrete: Materials, fabrication and properties, Compos. B Eng. 177 (2019) 107437.
- [4] K. Ramachandran, P. Vijayan, G. Murali, N.I. Vatin, A Review on Principles, Theories and Materials for Self Sensing Concrete for Structural Applications, Materials 15 (11) (2022) 3831.
- [5] E. Shamsaei, F.B. de Souza, X. Yao, E. Benhelal, A. Akbari, W. Duan, Graphene-based nanosheets for stronger and more durable concrete: A review, Constr. Build. Mater. 183 (2018) 642–660.
- [6] S. Dai Pang, H.J. Gao, C. Xu, S.T. Quek, H. Du, April. Strain and damage self-sensing cement composites with conductive graphene nanoplatelet, Sensors Smart Struct. Technol. Civil, Mech. Aerospace Syst. 9061 (2014) 546–556.
- [7] H. Du, S.T. Quek, S. Dai Pang, April. Smart multifunctional cement mortar containing graphite nanoplatelet, In Sensors and Smart Structures Technologies for Civil, Mechanical, and Aerospace Systems 8692 (2013) 871–880.
- [8] W. Dong, W. Li, K. Vessalas, X. He, Z. Sun, D. Sheng, Piezoresistivity deterioration of smart graphene nanoplate/cement-based sensors subjected to sulphuric acid attack, Compos. Commun. 23 (2021) 100563.
- [9] S. Sun, B. Han, S. Jiang, X. Yu, Y. Wang, H. Li, J. Ou, Nano graphite plateletsenabled piezoresistive cementitious composites for structural health monitoring, Constr. Build. Mater. 136 (2017) 314–328.
- [10] O. Sevim, Z. Jiang, O.E. Ozbulut, Effects of graphene nanoplatelets type on self-sensing properties of cement mortar composites, Constr. Build. Mater. 359 (2022) 129488.
- [11] G. Qi, Q. Wang, R. Zhang, Z. Guo, D. Zhan, S. Liu, Effect of rGO/GNP on the electrical conductivity and piezoresistance of cement-based composite subjected to dynamic loading, Constr. Build. Mater. 368 (2023) 130340.
- [12] A. Kausar, Z. Anwar, B. Muhammad, Recent developments in epoxy/graphite, epoxy/graphene, and epoxy/graphene nanoplatelet composites: a comparative review, Polym.-Plast. Technol. Eng. 55 (11) (2016) 1192–1210.
- [13] X.Y. Fang, X.X. Yu, H.M. Zheng, H.B. Jin, L. Wang, M.S. Cao, Temperature-and thickness-dependent electrical conductivity of few-layer graphene and graphene nanosheets, Phys. Lett. A 379 (37) (2015) 2245–2251.
- [14] A. Robin, E. Lhuillier, X.Z. Xu, S. Ithurria, H. Aubin, A. Ouerghi, et al., Engineering the charge transfer in all 2D graphene-nanoplatelets heterostructure photodetectors, Sci. Rep. 6 (1) (2016) 1–11.
- [15] A.D. Smith, F. Niklaus, A. Paussa, S. Vaziri, A.C. Fischer, M. Sterner, F. Forsberg, A. Delin, D. Esseni, P. Palestri, M. Östling, M.C. Lemme, Electromechanical piezoresistive sensing in suspended graphene membranes, Nano Lett. 13 (7) (2013) 3237–3242.
- [16] M. Cao, J. Su, S. Fan, H. Qiu, D. Su, L. Li, Wearable piezoresistive pressure sensors based on 3D graphene, Chem. Eng. J. 406 (2021) 126777.
- [17] ASTM C109/C109M-20 Standard Test Method for Compressive Strength of Hydraulic Cement Mortars (Using 2-in. or [50-mm] Cube Specimens).

- [18] ASTM C778-21 Standard Specification for Standard Sand.
- [19] E. Daş, S.A. Gürsel, L.I. Şanli, A.B. Yurtcan, Comparison of two different catalyst preparation methods for graphene nanoplatelets supported platinum catalysts, Int. J. Hydrogen Energy 41 (23) (2016) 9755–9761.
- [20] M.S. Konsta-Gdoutos, Z.S. Metaxa, S.P. Shah, Highly dispersed carbon nanotube reinforced cement based materials, Cem. Concr. Res. 40 (7) (2010) 1052–1059.
- [21] M.S. Konsta-Gdoutos, Z.S. Metaxa, S.P. Shah, Multi-scale mechanical and fracture characteristics and early-age strain capacity of high performance carbon nanotube/ cement nanocomposites, Cem. Concr. Compos. 32 (2) (2010) 110–115.
- [22] S. Bhattacharjee, DLS and zeta potential—what they are and what they are not? J. Control. Release 235 (2016) 337–351.
- [23] Y. Yao, Z. Lin, Z. Li, X. Song, K.S. Moon, C.P. Wong, Large-scale production of twodimensional nanosheets, J. Mater. Chem. 22 (27) (2012) 13494–13499.
- [24] ASTM C305-20 Standard Practice for Mechanical Mixing of Hydraulic Cement Pastes and Mortars of Plastic Consistency.
- [25] C. Backes, K.R. Paton, D. Hanlon, S. Yuan, M.I. Katsnelson, J. Houston, R.J. Smith, D. McCloskey, J.F. Donegan, J.N. Coleman, Spectroscopic metrics allow in situ measurement of mean size and thickness of liquid-exfoliated few-layer graphene nanosheets, Nanoscale 8 (7) (2016) 4311–4323.
- [26] P.A. Danoglidis, M.S. Konsta-Gdoutos, S.P. Shah, Relationship between the carbon nanotube dispersion state, electrochemical impedance and capacitance and mechanical properties of percolative nanoreinforced OPC mortars, Carbon 145 (2019) 218–228.
- [27] M.S. Konsta-Gdoutos, P.A. Danoglidis, S.P. Shah, Tailoring the piezoresistive sensing of CNT reinforced mortar sensors, Special Publication 335 (2019) 12–26.
- [28] ASTM C39/C39M Standard Test Method for Compressive Strength of Cylindrical Concrete Specimens.
- [29] G. He, Z. Yang, X. Zhou, J. Zhang, L. Pan, S. Liu, Polymer bonded explosives (PBXs) with reduced thermal stress and sensitivity by thermal conductivity enhancement with graphene nanoplatelets, Compos. Sci. Technol. 131 (2016) 22–31.

- [30] Y. Zhu, S. Murali, W. Cai, X. Li, J.W. Suk, J.R. Potts, R.S. Ruoff, Graphene and graphene oxide: synthesis, properties, and applications, Adv. Mater. 22 (35) (2010) 3906–3924.
- [31] D.G. Papageorgiou, I.A. Kinloch, R.J. Young, Mechanical properties of graphene and graphene-based nanocomposites, Prog. Mater Sci. 90 (2017) 75–127.
- [32] M. González-Hourcade, G. Simões dos Reis, A. Grimm, V.M. Dinh, E.C. Lima, S. H. Larsson, F.G. Gentili, Microalgae biomass as a sustainable precursor to produce nitrogen-doped biochar for efficient removal of emerging pollutants from aqueous media, J. Clean. Prod. 348 (2022) 131280.
- [33] B. Zhang, T. Chen, Study of ultrasonic dispersion of graphene nanoplatelets, Materials 12 (11) (2019) 1757.
- [34] J. Sato, Y. Takasu, K. Fukuda, W. Sugimoto, Graphene nanoplatelets via exfoliation of platelet carbon nanofibers and its electric double layer capacitance, Chem. Lett. 40 (1) (2011) 44–45.
- [35] F. Azhari, N. Banthia, Cement-based sensors with carbon fibers and carbon nanotubes for piezoresistive sensing, Cem. Concr. Compos. 34 (7) (2012) 866–873.
- [36] K. Sun, R. Fan, Y. Yin, J. Guo, X. Li, Y. Lei, L. An, C. Cheng, Z. Guo, Tunable negative permittivity with fano-like resonance and magnetic property in percolative silver/yittrium iron garnet nanocomposites, J. Phys. Chem. C 121 (13) (2017) 7564–7571.
- [37] M.S. Konsta-Gdoutos, C.A. Aza, Self sensing carbon nanotube (CNT) and nanofiber (CNF) cementitious composites for real time damage assessment in smart structures, Cem. Concr. Compos. 53 (2014) 162–169.
- [38] P.A. Danoglidis, M.S. Konsta-Gdoutos, E.E. Gdoutos, S.P. Shah, Strength, energy absorption capability and self-sensing properties of multifunctional carbon nanotube reinforced mortars, Constr. Build. Mater. 120 (2016) 265–274.
- [39] Y. Fan, M. Zhao, Z. Wang, X. Zhang, H. Zhang, Tunable electronic structures of graphene/boron nitride heterobilayers, Appl. Phys. Lett. 98 (8) (2011) 083103.
- [40] D.D.L. Chung, X. Xi, Piezopermittivity for capacitance-based strain/stress sensing, Sens. Actuators, A 332 (2021) 113028.